# Study of the Dehydration of $Co(H_2PO_4)_2 \cdot 2H_2O$

**Banjong Boonchom[†,‡] and Chanaiporn Danvirutai*[,§]**

King Mongkut's Institute of Technology Ladkrabang, Chumphon Campus, 17/1 M. 6 Pha Thiew District, Chumphon 86160, Thailand, Department of Chemistry, Faculty of Science, King Mongkut's Institute of Technology Ladkrabang, Bangkok 10520, Thailand, and Department of Chemistry, Faculty of Science, Khon Kaen University, Khon Kaen 40002, Thailand

The thermal transformation of $Co(H_2PO_4)_2 \cdot 2H_2O$ was studied under a dry air atmosphere using TG−DTG−DTA. The TG−DTG−DTA curves show that the transformation occurs in three steps, which are dehydration processes. $Co(H_2PO_4)_2 \cdot 2H_2O$ and its thermal transformation product were characterized by scanning electron microscopy (SEM), X-ray powder diffraction (XRD), Fourier transform infrared (FTIR), and UV−vis near-IR techniques. The nonisothermal kinetics of $Co(H_2PO_4)_2 \cdot 2H_2O$ was studied by means of the Kissinger method. The specificity of the thermal transformation was characterized by identification of the bonds to be selectively activated because of energy absorption at the vibrational level, which are confirmed by the comparison of calculated wavenumbers and observed wavenumbers of the FTIR spectra. The activated complex theory has been applied to each step of the reactions, and the thermodynamic functions $\Delta H^{\neq}$, $\Delta G^{\neq}$, and $\Delta S^{\neq}$ are calculated. These values for three stages showed that they are connected with the introduction of heat and are nonspontaneous processes.

## 1. Introduction

Currently, the acid phosphates of some bivalent metals have been reported to be important inorganic compounds.[1−5] They are generally known to possess optical, electrical, and magnetic properties of practical importance, which are determined by the presence of very strong hydrogen bonds in their crystal lattices.[5] In particular, manganese, iron, cobalt, nickel, and zinc dihydrogen phosphates are components of antiproof corrosion compositions.[2] Calcium, manganese, and iron dihydrogen phosphates are appropriate sources of macro- and micronutrients (P, Ca, Mn, Fe) because of their solubility in soil.[2] The dihydrate belongs to the well-known series of isostructural crystallohydrates $M(H_2PO_4)_2 \cdot 2H_2O$ (M = Mg, Mn, Co, Ni, Fe, Zn), which have similar X-ray diffraction patterns and close unit cell parameters. (They crystallize in the monoclinic space group $P2_1/n$ with $Z = 2$.)[1−5] $M(H_2PO_4)_2 \cdot 2H_2O$ can be synthesized from metal(II) carbonate and phosphoric acid at low temperature ((40 to 80) °C) over long time periods (> 8 h).[1] So far, only the crystal structure and thermal analysis of $M(H_2PO_4)_2 \cdot 2H_2O$ have been reported.[6,9,13,14] Most recently, Koleva et al. reported the crystal structure and magnetic properties of $M(H_2PO_4)_2 \cdot 2H_2O$ (M = Mg, Mn, Fe, Co, Ni, Zn, Cd).[1,5]The final decomposition products of metal dihydrogenphosphates were found to be metal cyclotetraphosphates, which are used as pigments, catalysts, and luminophore-supporting matrices.[6−9] Therefore, thermal treatments of these dihydrogen phosphate hydrates have a great synthetic potential, which relates to the hydrate in the conventional crystal form. The presence of water molecules influences the intermolecular interactions (affecting the internal energy and enthalpy) as well as the crystalline disorder (entropy) and, hence, influences the Gibbs energy, thermodynamic activity, solubility, stability, electrochemical, and catalytic activity.[10−14] To control the state of hydration of the active ingredient, it is therefore important and necessary to understand the kinetics and thermodynamics of dehydration and decomposition processes under appropriate conditions. In many methods of kinetics estimation, the model-free method is recommended to be a trustworthy way of obtaining reliable and consistent kinetic information,[10] which involves measuring the temperatures corresponding to fixed values of the extent of conversion ($\alpha$) from experiments at different heating rates ($\beta$). The results obtained on this basis can be directly applied to materials science for the preparation of various metals and alloys, ceramics, glasses, enamels, glazes, and polymer and composite materials.

In this respect, the formation of $Co_2P_4O_{12}$ from $Co(H_2PO_4)_2 \cdot 2H_2O$ was followed using differential thermal analysis−thermogravimetry (TG−DTG−DTA), X-ray powder diffraction (XRD), scanning electron microscopy (SEM), Fourier transform−infrared (FT-IR), and UV−vis near-IR techniques. Thermal transformation of $Co(H_2PO_4)_2 \cdot 2H_2O$ was studied by means of nonisothermal kinetics (the Kissinger method)[15] in which a correlation among the temperature, activation energy, and the wavenumbers assigned to the bond is responsible for the thermal decomposition steps of the compound. The relationship between kinetic parameters ($E$ and $A$) and thermodynamic functions ($\Delta H^{\neq}$, $\Delta G^{\neq}$, and $\Delta S^{\neq}$) via the Kissinger method is reported on the basis of thermal analysis techniques. This is an alternative method for the prediction of these parameters. The advantage of the Kissinger equation is that the values of $E$ and $A$ can be calculated on the basis of multiple thermogravimetric curves and do not require the selection of a particular kinetic model (type $g(\alpha)$ or $f(\alpha)$ function).[16,17] The thermodynamic ($\Delta H^{\neq}$, $\Delta S^{\neq}$, $\Delta G^{\neq}$) and kinetic ($E$ and $A$) parameters of three decomposition steps of $Co(H_2PO_4)_2 \cdot 2H_2O$ are discussed for the first time.

* Corresponding author. Tel: +66-43-202222 to 9 ext. 12243. Fax: +66-43-202373. E-mail: chanai@kku.ac.th.
† Chumphon Campus, King Mongkut's Institute of Technology Ladkrabang.
‡ Department of Chemistry, Faculty of Science, King Mongkut's Institute of Technology Ladkrabang.
§ Khon Kaen University.

10.1021/je800576w CCC: $40.75 
Published on Web 03/24/2009

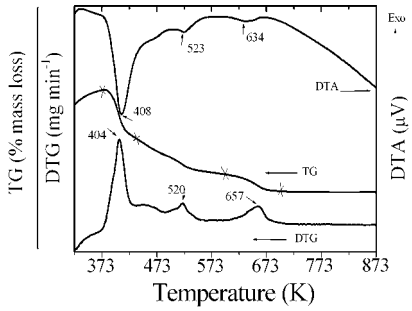


**Figure 1.** TG−DTG−DTA curves of $Co(H_2PO_4)_2 \cdot 2H_2O$ at a heating rate of 10 K·min$^{-1}$ in air.

## 2. Experimental Procedures

***2.1. Preparation.*** The compound $Co(H_2PO_4)_2 \cdot 2H_2O$ was prepared by a solution precipitation method using cobalt carbonate ($CoCO_3$, 99.99 %, Merck) and phosphoric acid (86.4 % w/w $H_3PO_4$, Merck) as starting materials. About 1.2*g* of $CoCO_3$was dissolved in 70 % $H_3PO_4$ (86.4 % w/w $H_3PO_4$ dissolved in DI water) with continuous stirring at 40 °C on a hot plate. The resulting solution was stirred until $CO_2$(g) was completely evolved ((15 to 30) min) and the precipitates were obtained. A nearly dry sample was obtained, and then 10 mL of acetone was added to allow a highly crystalline product to be developed. The prepared solid was filtered by a suction pump, washed with acetone, and dried in air.

***2.2. Characterization Methods.*** The water content was analyzed by TG data. Thermal properties of $Co(H_2PO_4)_2 \cdot 2H_2O$ were investigated on a TG−DTG−DTA apparatus (Pyris Diamond Perkin-Elmer Instruments). The experiments were performed under dynamic air at heating rates of (5, 10, 15, and 20) K·min$^{-1}$ over the temperature range from (303 to 873) K and the air flow rate of 100 mL·min$^{-1}$. A sample mass of about (6.0 to 10.0) mg was added to an alumina crucible without pressing. The thermogram of a sample was recorded in an open alumina crucible using α-$Al_2O_3$ as the reference material. The synthesized $Co(H_2PO_4)_2 \cdot 2H_2O$ was calcined in a box furnace at 773 K under air, and the thermal transformation products were further investigated. The structure and crystallite size of the prepared $Co(H_2PO_4)_2 \cdot 2H_2O$ and its thermal transformation product ($Co_2P_4O_{12}$) were studied by XRD using X-ray diffractometry (Phillips PW3040, The Netherlands) with Cu Kα radiation ($\lambda = 0.1546$ nm). The Scherrer method was used to evaluate the crystallite size (i.e., $D = K\lambda/\beta \cos \theta$, where $\lambda$ is the wavelength of X-ray radiation, $K$ is a constant taken to be 0.89, $\theta$ is the diffraction angle, and $\beta$ is the full width at half-maximum (fwhm)).[18] The morphologies of the selected resulting samples were examined by scanning electron microscope using a LEO SEM VP1450 after gold coating. The room temperature FTIR spectra were recorded in the range of (4000 to 370) cm$^{-1}$ with eight scans on a Perkin-Elmer Spectrum GX FT-IR/FT-Raman spectrometer with a resolution of 4 cm$^{-1}$ using KBr pellets (spectroscopy grade, Merck).

## 3. Result and Discussion

***3.1. Thermal Stability of $Co(H_2PO_4)_2 \cdot 2H_2O$.*** The TG−DTG−DTA curves of $Co(H_2PO_4)_2 \cdot 2H_2O$ are shown in Figure 1. The TG curve of $Co(H_2PO_4)_2 \cdot 2H_2O$ shows the weight loss in the range of (353 to 873) K. The observed increasing mass loss at the beginning of the TG curve may be due to the partial adsorbed moisture on the surface of the studied sample. The elimination of water was observed in three areas: (353 to 473) K, (473 to 573) K, and (573 to 703) K. The corresponding observed weight losses are (10.70, 7.27, and 4.76) % by mass, which correspond to (1.72, 1.17, and 0.76) mol of water, respectively. Three endothermic effects on the DTA are observed at (408, 523, and 634) K, which correspond to the DTG peaks at (404, 520, and 657) K, respectively. The thermal decomposition of $Co(H_2PO_4)_2 \cdot 2H_2O$ is a complex process, that involves the dehydration of the coordinated water molecules (∼2 mol $H_2O$) in the first step and an intramolecular dehydration of the protonated phosphate groups (∼2 mol $H_2O$) in the last two steps. The processes can be formally presented as

$$Co(H_2PO_4)_2 \cdot 2H_2O \rightarrow Co(H_2PO_4)_2 + {\sim}2H_2O \quad (1)$$

$$Co(H_2PO_4)_2 \rightarrow CoH_2P_2O_7 + {\sim}H_2O \quad (2)$$

$$CoH_2P_2O_7 \rightarrow {}^1/_2Co_2P_4O_{12} + {\sim}H_2O \quad (3)$$

A large number of intermediate compounds, such as acid polyphosphate, $Co(H_2PO_4)_2$, acid condensed phosphate, $CoH_2P_2O_7$, and mixtures of intermediates of both have been registered. Cobalt cyclotetraphosphate, $Co_2P_4O_{12}$, was found to be the final product of the thermal transformation in the range of (673 to 873) K, as revealed by the TG curve. The total mass loss is 22.73 % (3.64 mol $H_2O$), which is close to the theoretical value (24.92 % (4 mol $H_2O$) and is also in agreement with those values reported in the literature to be in the range of 1 to 4).[1−5] To gain the complete dehydration of synthesized $Co(H_2PO_4)_2 \cdot 2H_2O$, the sample of $Co(H_2PO_4)_2 \cdot 2H_2O$ was heated in the furnace at 773 K for 3 h, and the dehydrated product was found to be cobalt cyclotetraphosphate, $Co_2P_4O_{12}$.

The specificity of the thermal decomposition was characterized by identification of the bonds to be selectively activated because of energy absorption at the vibrational level.[13] We assigned these bonds by comparing the calculated wavenumbers with the observed wavenumbers in the IR spectra. The specificity of decomposition under nonisothermal conditions is due to a selective vibrational energy accumulation on a certain bond. This breaking bond is assimilated with a Morse oscillator[19] coupled nonlinear to the harmonic oscillators of the thermic field. Following a theoretical treatment developed by Vlase et al.,[13] the relationship between the isokinetic temperature ($T_i$) and the wavenumber of the activated bond is

$$\omega_{calcd} = \frac{k_B}{hc} T_i = 0.695 T_i \quad (4)$$

$k_B$ and $h$ are, respectively, the Boltzmann and Planck constants, and $c$ is the light velocity. Because the breaking bond has an unharmonic behavior, the specific activation is possible due to more than one quanta or a higher harmonic. Here, $\omega_{calcd}$ is calculated by eq 4, which is assigned to the spectroscopic wavenumber for the bond supposed to break. $\omega_{sp}$ is the frequency band of a particular vibrational mode and is calculated by $\omega_{sp} = q\omega_{calcd}$, $q \in N = 1, 2, 3, \ldots$ (quanta number). Additionally, the $\omega_{calcd}$ values with the $\omega_{sp}$ values determined from the DTG data, together with the assignments of the corresponding oscillations, are compared. In this article, we suggested the maximum peak temperature, $T_p$, in the DTG curve for the calculated wavenumbers ($\omega_{sp}$) according to eq 4. To corroborate the calculated data with the spectroscopic data, we drew up the FTIR spectra of the studied compound. Table 1

**Table 1. Kinetic Parameters and FTIR Band Assignments**

| step | temp (K) in four heating rates $\beta$/K·min$^{-1}$ 5 | 10 | 15 | 20 | average $T_p$ K | $E_a$ kJ·mol$^{-1}$ | $r^2$ | $q$ | n$\omega$ cm$^{-1}$ | FTIR band assignments |
|---|---|---|---|---|---|---|---|---|---|---|
| 1 | 393.15 | 398.15 | 401.15 | 403.45 | 398.98 | 171.43 ± 1.63 | 0.99991 | 6 | 1663 | $\nu_2$ ($H_2O$) |
| | | | | | | | | 12 | 3327 | $\nu_1$ ($H_2O$) |
| | | | | | | | | 13 | 3604 | $\nu_3$ ($H_2O$) |
| 2 | 505.36 | 512.39 | 516.97 | 520.03 | 513.69 | 197.24 ± 2.52 | 0.99984 | 2 | 714 | $\gamma_{OH}$ ($H_2PO_4^-$) |
| | | | | | | | | 3 | 1071 | $\nu(PO_2)$ |
| | | | | | | | | 5 | 1785 | band C ($H_2PO_4^-$ |
| | | | | | | | | 7 | 2499 | band B ($H_2PO_4^-$) |
| | | | | | | | | 9 | 3213 | band A ($H_2PO_4^-$) |
| 3 | 621.15 | 635.99 | 647.65 | 654.15 | 639.74 | 129.24 ± 5.20 | 0.99839 | 1 | 444 | $\delta$ ($O_2PO_2$) |
| | | | | | | | | 2 | 889 | $\nu$ ($PO_2(H_2)$ |
| | | | | | | | | 4 | 1778 | band C ($H_2PO_4^-$ |

shows the comparison of the $\omega_{calcd}$ values with the $\omega_{sp}$ values determined from this compound, together with the assignments of the corresponding vibrational modes in the literature.[19,20] These thermal decomposition kinetics were studied in three mass loss steps, which correspond to the loss of coordinated water (the first step), followed by a continuous intermolecular polycondensation and elimination of water (two last steps). The studied compound exhibited a very good agreement between the calculated wavenumbers from average $T_p$ (DTG) and the observed wavenumbers from IR spectra for the bonds suggested to be broken. Therefore, the use of $T_p$ (DTG) will be an alternative method for calculating the wavenumbers for identification in each thermal transition step of interesting materials.

***3.2. Characterization Results. 3.2.1. X-ray Powder Diffraction.*** The XRD patterns of $Co(H_2PO_4)_2\cdot 2H_2O$ and its decomposition product $Co_2P_4O_{12}$ are shown in Figure 2. All detectable peaks of the $Co(H_2PO_4)_2\cdot 2H_2O$ and $Co_2P_4O_{12}$ are indexed as $Co(H_2PO_4)_2\cdot 2H_2O$ and $Co_2P_4O_{12}$ structures, which are identified using the standard data of PDF nos. 390698 and 842208, respectively. These results indicated that the two crystal structures are in the monoclinic system with space group $P2_1/n$ ($Z = 2$) for $Co(H_2PO_4)_2\cdot 2H_2O$ and $C2/c$ ($Z = 4$) for $Co_2P_4O_{12}$. The average crystallite sizes and lattice parameters of $Co(H_2PO_4)_2\cdot 2H_2O$ and $Co_2P_4O_{12}$ were calculated from X-ray spectra and are tabulated in Table 2. The lattice parameters of $Co(H_2PO_4)_2\cdot 2H_2O$ and $Co_2P_4O_{12}$ are compared with those of the standard data of PDF nos. 390698 and 842208, respectively.

***3.2.2. Vibrational Spectroscopy.*** The FTIR spectra of $Co(H_2PO_4)_2\cdot 2H_2O$ and $Co_2P_4O_{12}$ are shown in Figure 3 and are very similar to those of $M(H_2PO_4)_2\cdot 2H_2O$ and $M_2P_4O_{12}$ (where M = Mn, Co, Ni).[1−6] Vibrational bands are identified in relation to the crystal structure in terms of the fundamental vibrating units, namely, $H_2PO_4^-$ and $H_2O$ for $Co(H_2PO_4)_2\cdot 2H_2O$ and the $[P_4O_{12}]^{4-}$ ion for $Co_2P_4O_{12}$, which are assigned according to the literature.[21,22] Vibrational bands of the $H_2PO_4^-$ ion are

**Table 2. Average Crystallite Sizes and Lattice Parameters of $Co(H_2PO_4)_2\cdot 2H_2O$ and $Co_2P_4O_{12}$ Calculated from XRD Data**

| compd | method | $a$/Å | $b$/Å | $c$/Å | $\beta$/deg | average crystallite sizes/nm |
|---|---|---|---|---|---|---|
| $Co(H_2PO_4)_2\cdot 2H_2O$ | PDF no. 390698 | 7.27 | 9.88 | 5.33 | 94.86 | |
| | This work | 7.21(3) | 9.91(1) | 5.29(5) | 94.88(6) | 26 ± 2 |
| $Co_2P_4O_{12}$ | PDF no. 842208 | 11.8 | 8.28 | 9.92 | 118.72 | |
| | this work | 11.83(8) | 8.22(6) | 9.94(0) | 118.51(1) | 40 ± 10 |

observed in the regions of (300 to 500) cm$^{-1}$, (700 to 900) cm$^{-1}$, (1160 to 900) cm$^{-1}$, (840 to 930) cm$^{-1}$, (1000 to 1200) cm$^{-1}$, and (2400 to 3300) cm$^{-1}$. These bands are assigned to the $\delta(O_2PO_2)$, $\gamma$(POH), $\delta$(POH), $\nu(PO_2(H_2))$, $\nu(PO_2)$, and $\nu_{OH}$ of $H_2O$ molecules and $H_2PO_4^-$ ions, respectively. The observed bands in the (1600 to 1700) cm$^{-1}$ and (3000 to 3500) cm$^{-1}$ region are attributed to the water bending/C band and stretching vibrations/A band, respectively. Vibrational bands of the $[P_4O_{12}]^{4-}$ ion are observed in the ranges of (1350 to 1220) cm$^{-1}$, (1150 to 1100) cm$^{-1}$, (1080 to 950) cm$^{-1}$, and (780 to 400) cm$^{-1}$. These bands can be assigned to $\nu_{as}OPO^-$, $\nu_sOPO^-$, $\nu_{as}$POP, and $\nu_s$POP vibrations, respectively.[21] The observation of a strong $\nu_s$POP band is known to be the most striking feature of the cyclotetraphosphate spectra, along with the presence of the $\nu_{as}OPO^-$ band. The FTIR results are consistent with the XRD data (Figure 2).

***3.2.3. Scanning Electron Microscopy.*** The SEM micrographs of the synthetic $Co(H_2PO_4)_2\cdot 2H_2O$ and its decomposition product $Co_2P_4O_{12}$ show the nonuniform morphological features (Figure 4). The SEM micrograph of $Co(H_2PO_4)_2\cdot 2H_2O$ consists of nonuniform spherical grains, which contain microparticles having a distribution of small particles ((2 to 8) $\mu$m) and large particles ((> 10 to 100) $\mu$m) (Figure 4a). The SEM micrograph of $Co_2P_4O_{12}$ shows a porous structure and agglomeration; the

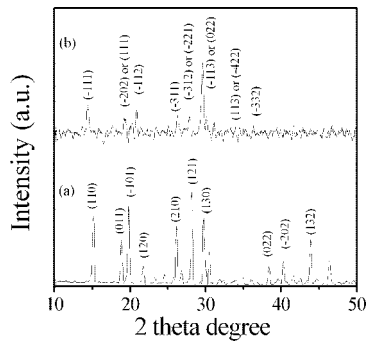


**Figure 2.** XRD patterns of (a) $Co(H_2PO_4)_2\cdot 2H_2O$ and (b) its dehydration product $Co_2P_4O_{12}$.

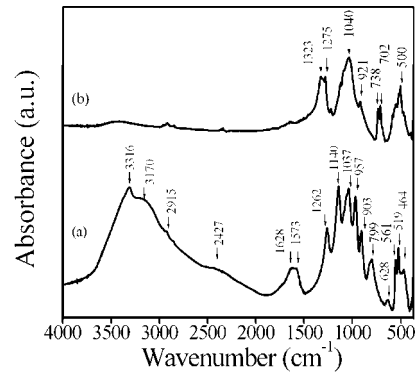


**Figure 3.** FTIR spectra of (a) $Co(H_2PO_4)_2\cdot 2H_2O$ and (b) its dehydration product $Co_2P_4O_{12}$.

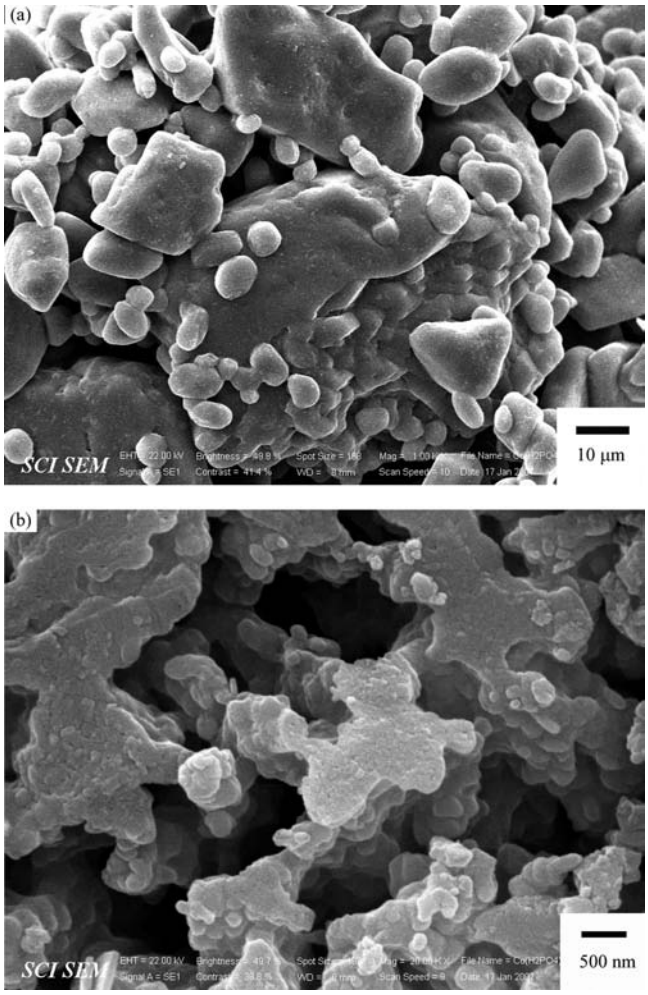


**Figure 4.** SEM micrographs of (a) $Co(H_2PO_4)_2 \cdot 2H_2O$ and (b) its dehydration product $Co_2P_4O_{12}$.

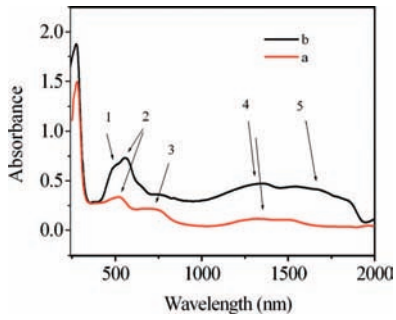


**Figure 5.** UV−vis near-IR spectra of (a) $Co(H_2PO_4)_2 \cdot 2H_2O$ and (b) its dehydration product $Co_2P_4O_{12}$.

appearance of micropores ((100 to 400) nm) and macropores ((500 to 2000) nm) is due to the process of thermal decomposition (Figure 4b). The different porous sizes of $Co_2P_4O_{12}$ are primarily caused by dehydration processes, which relate to an intermolecular dehydration of the protonated dihydrogen phosphate groups. The results may be potentially useful for catalyst application because the catalytic activity of $Co_2P_4O_{12}$ significantly varies with the method of precipitation, thermal treatment, and porous structure on the surface.

***3.2.4. Ultraviolet−Visible Near-Infrared Spectroscopy.*** The UV−vis near-IR absorption spectrum of $Co(H_2PO_4)_2 \cdot 2H_2O$ is shown in Figure 5a and shows that the dominant feature of $Co^{2+}$ in octahedral sites is too weak to be observed because it involves spin-forbidden transitions. The absorption bands of

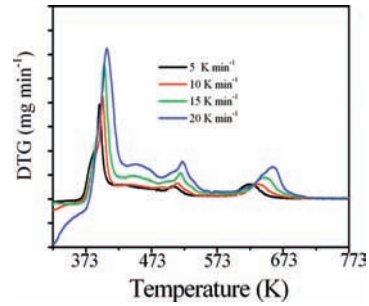


**Figure 6.** DTG curves of $Co(H_2PO_4)_2 \cdot 2H_2O$ at four different heating rates in air (5, 10, 15, and 20 $K \cdot min^{-1}$).

$Co(H_2PO_4)_2 \cdot 2H_2O$ powder are observed and labeled as 1, 2, 3, and 4 around wavelengths of (472, 563, 696, and 1200 to 1400) nm, respectively. The results indicate that $Co^{2+}$ exists in a distorted octahedral site in the structure (Jahn−Teller effect; extensively discussed previously).[5,8,23,24] The band around 255 nm is too strong to be a d-d transition, lying in the UV region; it is assigned to a charge-transfer band. In six-coordinate, high-spin Co(II) complexes, a band near (1440 to 1000) nm can be assigned to the $^4T_{1g} \rightarrow {}^4T_{2g}$ transition. In addition, a multiple structured band, assigned to $^4T_{1g} \rightarrow {}^4T_{1g}(P)$, is seen in the visible region near 500 nm, which is split into two components ((472 and 563) nm). The weak absorption at 696 nm is due to the $^4T_{1g} \rightarrow {}^4A_{2g}$ transition. Figure 5b shows the UV−vis near-IR spectra of the $Co_2P_4O_{12}$ compound. Co(II) in octahedral sites is present in this structure.[24] The spectral feature of the octahedral site in $Co_2P_4O_{12}$ appears at (513 (1), 563 (2), 753 (3), and 1328 (4)) nm (peak numbers are given in parentheses). These absorption bands are assigned to $^4T_{1g} \rightarrow {}^4T_{2g}(P)$ transition for a multiple structure band ((513 and 563) nm), whereas the observed absorption bands at ca. (753 and 1328) nm are attributed to the $^4T_{1g} \rightarrow {}^4A_{2g}$ and $^4T_{1g} \rightarrow {}^4T_{2g}$ transitions, respectively.[5,8,23,24]

***3.3. Kinetic and Thermodynamic Studies.*** The activation energies for the thermal transformation steps of $Co(H_2PO_4)_2 \cdot 2H_2O$ were calculated from three endothermic DTG peaks (Figure 6). Several nonisothermal techniques have been proposed that are quicker and less sensitive to previous and next transformations.[10−15] In addition, they can provide the more accurate activation energy and crystal growth mode. Nonisothermal data are typically interpreted using the Kissinger equation[15]

$$\ln\left(\frac{\beta}{T_p^2}\right) = \ln\left(\frac{E}{RA}\right) - \left(\frac{E}{RT_p}\right) \quad (5)$$

Here $\beta$ is the heating rate of the TG curve ($K \cdot min^{-1}$), and the DTG curve is the differential form of the TG curve. $E_a$ is the activation energy for the phase transformation ($kJ \cdot mol^{-1}$), $R$ is the gas constant (8.314 $J \cdot mol^{-1} \cdot K^{-1}$), and $T_p$ is the average phase transformation temperature peak in the DTG curve (K). In previous work, it is common for the $T_p$ values for various heating to be precisely evaluated from nonisothermal data (DTA, DTG, or DSC curves) conferred to the Kissinger method to evaluate the kinetic parameters.[10−17] In this present work, plots of $\ln(\beta/T^2)$ versus $1/T_p$ should give straight lines with the values of the activation energy and pre-exponential factor given by the slope and the intercept for the different decomposition stages of $Co(H_2PO_4)_2 \cdot 2H_2O$. Figure 7 shows the Kissinger plots of the three decomposition steps of the prepared $Co(H_2PO_4)_2 \cdot 2H_2O$ sample. From the slopes of the curves, the activation energy

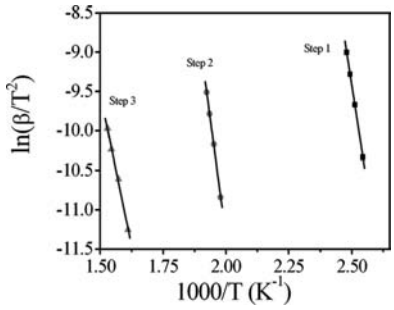


**Figure 7.** KAS analysis of three decomposition steps of $Co(H_2PO_4)_2 \cdot 2H_2O$ at four different heating rates in air [(5, 10, 15, and 20) $K \cdot min^{-1}$].

values of the prepared $Co(H_2PO_4)_2 \cdot 2H_2O$ sample in the three steps were calculated to be (171.43 ± 1.63, 197.24 ± 2.52, and 129.24 ± 5.20) $kJ \cdot mol^{-1}$, respectively (Table 1). The water in the crystalline hydrate may be considered to be either water of crystallization (crystal water) or coordinated water. The activation energy for the release of the water of crystallization lies in the range of (60 to 80) $kJ \cdot mol^{-1}$, whereas the values for coordinately bound water activation energy are within the range of (120 to 160) $kJ \cdot mol^{-1}$.[14] In addition, the water eliminated at 423 K and below can be considered to be water of crystallization, whereas water eliminated at 473 K and above indicates its coordination by the metal atom.[11−14] The calculated activation energies from the Kissinger method for the three dehydration reactions suggest that the water molecules are coordinated for all decomposition steps. These activation energies are related to the vibrational frequencies and are an indication of the energy of the bond breaking of intermediate species. The second step exhibits higher activation energy in comparison with other steps, and this is understandable because this step corresponds to a true P−OH bond breaking, in connection with a polycondensation reaction.[4] The lowest activation energy in the last step indicates the instability of the intermediate compounds ($Co(H_2PO_4)_2$, $CoH_2P_2O_7$, and mixtures of both intermediates) before transformation to $Co_2P_4O_{12}$. This result is inconsistent with TG−DTG−DTA data, as shown in eqs 2 and 3.

The pre-exponential factor ($A$) values can be estimated from the intercept of the plots of eq 5. The pre-exponential factor ($A$) values in the Arrhenius equation for solid-phase reactions are expected over a wide range (six or seven orders of magnitude), even after the effect of surface area is taken into account.[25−28] Low factors will often indicate a surface reaction, but if the reactions are not dependent on surface area, then the low factor may indicate a "tight" complex. High factors will usually indicate a "loose" complex.[25] Even higher factors (after correction for surface area) can be obtained for complexes having free translation on the surface. Because concentrations in solids are not controllable in many cases, it would have been convenient if the magnitude of the pre-exponential factor indicated reaction molecularity. On the basis of these reasons, three steps of the thermal decomposition of $Co(H_2PO_4)_2 \cdot 2H_2O$ may be interpreted to be loose complexes. The last step exhibits a lower pre-exponential factor ($A$) in comparison with that of the other steps, and this is consistent with the results of the activation energy value and TG−DTG−DTA.

From the activated complex theory (transition state) of Eyring,[25−28] the following general equation may be written

$$A = \left(\frac{e\chi k_B T_p}{h}\right) \exp\left(\frac{\Delta S^{\neq}}{R}\right) \quad (6)$$

**Table 3. Values of $\Delta S^{\neq}$, $\Delta H^{\neq}$, and $\Delta G^{\neq}$ for Three Decomposition Steps of $Co(H_2PO_2)_4 \cdot 2H_2O$**

| parameter | 1st step | 2nd step | 3rd step |
|---|---|---|---|
| $A$ ($s^{-1}$) | $1.71 \cdot 10^{22}$ | $6.42 \cdot 10^{19}$ | $3.67 \cdot 10^{9}$ |
| $\Delta S^{\neq}$ ($J \cdot mol^{-1} \cdot K^{-1}$) | 169.98 | 121.44 | −76.47 |
| $\Delta H^{\neq}$ ($kJ \cdot mol^{-1}$) | 168.13 | 192.97 | 123.92 |
| $\Delta G^{\neq}$ ($kJ \cdot mol^{-1}$) | 100.31 | 130.59 | 172.85 |

where $e = 2.7183$ is the Neper number, $\chi$ is the transition factor, which is unity for monomolecular reactions, $k_B$ is the Boltzmann constant, $h$ is the Planck constant, and $T_p$ is the average peak temperature of four DTG curves at four heating rates (Table 1). The change of the entropy may be calculated according to the formula

$$\Delta S^{\neq} = R \ln\left(\frac{Ah}{e\chi k_B T_p}\right) \quad (7)$$

because

$$\Delta H^{\neq} = E^{\neq} - RT_p \quad (8)$$

when $E^{\neq}$ is the activation energy from the Kissinger method. The enthalpy $\Delta H^{\neq}$ and Gibbs energy $\Delta G^{\neq}$ for the activated complex formation from the reagent can be calculated using the well-known thermodynamics equation

$$\Delta G^{\neq} = \Delta H^{\neq} - T_p \Delta S^{\neq} \quad (9)$$

On the basis of the values of activation energy ($E$) and pre-exponential factor ($A$) for different stages of decomposition calculated, the values of $\Delta S^{\neq}$, $\Delta H^{\neq}$, and $\Delta G^{\neq}$ for the formation of the activated complex from the reagent calculated according eqs 6, 7, 8, and 9 are presented in Table 3.

As can be seen from Table 3, the entropy of activation ($\Delta S^{\neq}$) values for the first and second steps are positive. This means that the corresponding activated complexes have a lower degree of arrangement (higher entropy) than the initial state, whereas, for the third stage, this is vice versa. Because the decomposition of $Co(H_2PO_4)_2 \cdot 2H_2O$ proceeds as three consecutive reactions, the formation of the second and third activated complexes passed in situ. Obviously, the entropy of the third activated complex was lower than that of the preceding complex (indicated by the negative value of $\Delta S^{\neq}$), whereas that of the second complex was higher and the value of $\Delta S^{\neq}$ was positive. In terms of the activated complex theory (transition theory),[25−28] a positive value of $\Delta S^{\neq}$ indicates a malleable activated complex that leads to a large number of degrees of freedom of rotation and vibration. A result may be interpreted to be a "fast" stage. However, a negative value of $\Delta S^{\neq}$ indicates a highly ordered activated complex, and the degrees of freedom of rotation as well as of vibration are less than they are in the nonactivated complex. The result may indicate a "slow" stage.[25] On the basis of these results, the first and second stages of the thermal decomposition of $Co(H_2PO_4)_2 \cdot 2H_2O$ may be interpreted to be "fast" stages, whereas the third stage can interpreted to be a "slow" stage. The highest values of $\Delta H^{\neq}$ and $\Delta G^{\neq}$ in the second step confirm the breaking of strong hydrogen-bonded P−OH groups in this structure. These results are consistent with the estimated activation energy and DTG and DTA data. The positive values of the enthalpy, $\Delta H^{\neq}$ and $\Delta G^{\neq}$, for all stages are in good agreement with three endothermic effects in the

DTA data, which indicate that they are connected to the introduction of heat and they are nonspontaneous processes.

## 4. Conclusions

$Co(H_2PO_4)_2 \cdot 2H_2O$ decomposes in three steps, which relate the dehydration reactions of crystal water and deprotonated hydrogen phosphate groups, and its decomposition product is cobalt cyclo-tetraphosphate ($Co_2P_4O_{12}$). The XRD, FTIR, and UV−vis-near-IR results confirmed the formation of $Co(H_2PO_4)_2 \cdot 2H_2O$ and $Co_2P_4O_{12}$ compounds. Thermal kinetic study results indicate the activation energies, which are related to vibrational frequencies of breaking bond of thermal transformation of $Co(H_2PO_4)_2 \cdot 2H_2O$. The thermal behavior, morphologies, and particle sizes of $Co(H_2PO_4)_2 \cdot 2H_2O$ and its thermal transformation product, ($Co_2P_4O_{12}$), show interesting features of some physical and chemical properties. These materials may be useful for many potential applications including catalytic, ceramic dye pigment, and magnetic materials. The values of the apparent activation energy and pre-exponential factor and the changes of entropy, enthalpy, and Gibbs energy can be calculated using DTG data based on the Kissinger method, of which certain conclusions can be made concerning the mechanisms and characteristics of the processes. The data of kinetics and thermodynamics play an important role in theoretical study, application development, and industrial production of the studied compound. Therefore, these data will be important for further studies of the studied compounds, which can solve various scientific and practical problems involving the participation of solid phases.

### Acknowledgment

We thank the Chemistry and Physics Departments, Khon Kaen University for providing research facilities.

### Supporting Information Available:

$Co(H_2PO_4)_2 \cdot 2H_2O$ and $Co_2P_4O_{12}$ standard data. This material is available free of charge via the Internet at http://pubs.acs.org.

## Literature Cited

(1) Koleva, V.; Mehandjiev, D. Characterization of $M(H_2PO_4)_2 \cdot 2H_2O$ (M = Mn, Co, Ni) and their in situ thermal decomposition by magnetic measurements. *Mater. Res. Bull.* **2006**, 41–469.
(2) Antraptseva, N. M.; Shchegrov, L. N.; Ponomareva, I. G. Thermolysis features of manganese(II) and zinc dihydrogenphosphate solid solution. *Russ. J. Inorg. Chem.* **2006**, 51–1493.
(3) Danvirutai, C.; Boonchom, B.; Youngme, S. Nanocrystalline manganese dihydrogen phosphate dihydrate $Mn(H_2PO_4)_2 \cdot 2H_2O$ and its decomposition product ($Mn_2P_4O_{12}$) obtained by simple precipitation route. *J. Alloys Compd.* **2008**, *457*, 75.
(4) Boonchom, B.; Maensiri, S.; Danvirutai, C. Soft solution synthesis, non-isothermal decomposition kinetics and characterization of manganese dihydrogen phosphate dihydrate $Mn(H_2PO_4)_2 \cdot 2H_2O$ and its thermal transformation products. *Mater. Chem. Phys.* **2008**, 109–404.
(5) Koleva, V.; Effenberger, H. Crystal chemistry of $M[PO_2(OH)_2]_2 \cdot 2H_2O$ compounds (M = Mg, Mn, Fe, Co, Ni, Zn, Cd): structural investigation of the Ni, Zn, and Cd salts. *J. Solid State Chem.* **2007**, 180–966.
(6) Lukyanchenko, O. A.; Samuskevich, V. V. Thermal transformations of $Co(H_2PO_4)_2 \cdot 2H_2O$. *Thermochim. Acta* **1999**, *327*, 181.
(7) Trojan, M.; Brandová, D.; Sŏlc, Z. Study of the thermal preparation and stability of tetrametaphosphates of bivalent metals. *Thermochim. Acta* **1987**, 110–343.
(8) Gunsser, W.; Fruehauf, D.; Rohwer, K.; Zimmermann, A.; Wiedenmann, A. Synthesis and magnetic properties of transition metal cyclotetraphosphates $M_2P_4O_{12}$ (M = Mn, Co, Ni, Cu). *J. Solid State Chem.* **1989**, 82–43.
(9) Trojan, M.; Brandová, D.; Sŏlc, Z. Reaction of formation of *c*-$Co_2P_4O_{12}$, a study using thermal analysis methods. *Thermochim. Acta* **1985**, 85–99.
(10) Vlaev, L. T.; Nikolova, M. M.; Gospodinov, G. G. Non-isothermal kinetics of dehydration of some selenite hexahydrates. *J. Solid State Chem.* **2004**, *177*, 2663.
(11) Zhang, K.; Hong, J.; Cao, G.; Zhan, D.; Tao, Y.; Cong, C. The kinetics of thermal dehydration of copper(II) acetate monohydrate in air. *Thermochim. Acta* **2005**, *437*, 145.
(12) Gao, X.; Dollimore, D. A kinetic study of the thermal decomposition of manganese(II) oxalate dehydrate. *Thermochim. Acta* **1993**, *215*, 47.
(13) Vlase, T.; Vlase, G.; Doca, M.; Doca, N. Specificity of decomposition of solids in non-isothermal conditions. *J. Therm. Anal. Calorim.* **2003**, *72*, 597.
(14) Gabal, M. A. Kinetics of the thermal decomposition of $CuC_2O_4$−$ZnC_2O_4$mixture in air. *Thermochim. Acta* **2003**, *402*, 199.
(15) Kissinger, H. E. Reaction kinetics in differential thermal analysis. *Anal. Chem.* **1957**, *29*, 1702.
(16) Mianowski, A.; Bigda, R. The Kissinger law and isokinetic effect. Part II. Experimental analysis. *J. Therm. Anal. Calorim.* **2004**, *75*, 355.
(17) Mohamed, M. A.; Galwey, A. K.; Halawy, S. A. Kinetic and thermodynamic study of the non-isothermal decomposition of cobalt malonate dihydrate and of cobalt hydrogen malonate dehydrate. *Thermochim. Acta* **2000**, *346*, 91.
(18) Cullity, B. D. *Elements of X-ray Diffraction*, 2nd ed.; Addison-Wesley Publishing: Reading, MA, 1977.
(19) Herzberg, G. *Zweiatomige Moleküle*; Molekülspektren und Molekülstruktur, Vol. 1; Steinkopff: Dresden, Germany. 1939.
(20) Colthup, N. B.; Daly, L. H.; Wiberley, S. E. *Introduction to Infrared and Raman Spectroscopy*; Academic Press: New York, 1964.
(21) Ramakrishnan, V.; Aruldhas, G.; Bigotto, A. Vibrational spectra of Cu(II) and Co(II) tetrametaphosphates. *Infrared Phys.* **1985**, 25–665.
(22) Soumhi, E. H.; Saadoune, I.; Driss, A. A new organic-cation cyclotetraphosphate $C_{10}H_{28}N_4P_4O_{12} \cdot 4H_2O$: crystal structure, thermal analysis, and vibrational spectra. *J. Solid State Chem.* **2001**, 156–364.
(23) Aranda, M. A. G.; Bruque, S. Characterization of manganese(III) orthophosphate hydrate. *Inorg. Chem.* **1990**, 29–1334.
(24) Tusar, N. N.; Mali, G.; Arčon, I.; Kaučič, V.; Ghanbari-Siahkali, A.; Dwyer, J. Framework cobalt and manganese in MeAPO-31 (Me = Co, Mn) molecular sieves. *Microporous Mesoporous Mater.* **2002**, 55–203.
(25) Cordes, H. M. Preexponential factors for solid-state thermal decomposition. *J. Phys. Chem.* **1968**, *72*, 2185.
(26) Criado, J. M.; Pérez-Maqueda, L. A.; Sánchez-Jiménez, P. E. Dependence of the preexponential factor on temperature. *J. Therm. Anal. Calorim.* **2005**, *82*, 671.
(27) Ŝesták, J. *Thermophysical Properties of Solids: Their Measurements and Theoretical Thermal Analysis*; Elsevier: New York, 1984.
(28) Young, D. A. *Decomposition of Solids*, 1st ed.; Pergamon Press: Oxford, U.K., 1966.

Received for review July 25, 2008. Accepted February 7, 2009. This work is financially supported by King Mongkut's Institute of Technology Ladkrabang (KMITL) and the Center of Excellence for Innovation in Chemistry (PERCH-CIC), Commission on Higher Education, Ministry of Education, Thailand.

JE800576W